Geological Magazine

www.cambridge.org/geo

Original Article

Cite this article: Osés GL, Afonso JWL, Wood RA, Freitas BT, Romero GR, Paula-Santos GM, Caetano-Filho S, Pacheco MLAF, Rodrigues CL, Silva TF, and Amorim KB. Clastic sedimentary record impacted by carbonate bioclasts in the Late Ediacaran. *Geological Magazine* **162**(e2): 1–13. https://doi.org/10.1017/S0016756824000335

Received: 16 April 2024
Revised: 20 September 2024
Accepted: 29 September 2024

Keywords:
Late Ediacaran; Bioclasts; Siliciclastic settings; *Corumbella*

Corresponding author:
Mírian L A F Pacheco;
Email: forancelli.ufscar@gmail.com

Clastic sedimentary record impacted by carbonate bioclasts in the Late Ediacaran

Gabriel L Osés[1,2], Jhon W L Afonso[3], Rachel A Wood[4], Bernardo T Freitas[5], Guilherme R Romero[6], Gustavo M Paula-Santos[7], Sergio Caetano-Filho[8], Mírian L A F Pacheco[9], Cleber L Rodrigues[10], Tiago F Silva[10] and Kamilla B Amorim[11]

[1]Programa de Pós-Graduação em Ecologia e Recursos Naturais, Universidade Federal de São Carlos, São Carlos, Brazil; [2]Laboratório de Arqueometria e Ciências Aplicadas ao Patrimônio Cultural, Instituto de Física, Universidade de São Paulo, São Paulo, Brazil; [3]Observatório Nacional, Rio de Janeiro, Brazil; [4]School of GeoSciences, University of Edinburgh, Edinburgh, UK; [5]Faculdade de Tecnologia, Universidade Estadual de Campinas, Limeira, Brazil; [6]Instituto de Geociências, Universidade de São Paulo, São Paulo, Brazil; [7]Faculty of Geosciences and MARUM, University of Bremen, Bremen, Germany; [8]Instituto de Geociências e Ciências Exatas, Universidade Estadual Paulista, Rio Claro, Brazil; [9]Laboratório de Paleobiologia e Astrobiologia, Universidade Federal de São Carlos, Sorocaba, Brazil; [10]Instituto de Física, Universidade de São Paulo, São Paulo, Brazil and [11]Faculdade de Geociências, Universidade Federal de Mato Grosso, Cuiabá, Brazil

Abstract

Clastic sedimentary systems and their characteristics are assumed not to have been modified by carbonate bioclastic grains until the Phanerozoic. Here, we show that the presence of carbonate bioclasts produced by disintegrated biomineralizing metazoans modified fine-grained siliciclastic facies in the Late Ediacaran Tamengo Formation, Brazil, ca. 555–542 Ma. The analysis of both polished sections and thin sections shows that sand-sized carbonate bioclasts (< 2 mm) derived from the Ediacaran metazoan *Corumbella* created diverse sedimentary features later found in the Phanerozoic record, such as bioclastic-rich horizontal and low-angle cross-laminations, erosive pods and lenses, bioclastic syneresis cracks, ripples preserved by bioclastic caps, microbial lamination eroded and filled with bioclasts, and entrapped bioclasts within microbial mats. These sedimentary features would have hardly been recorded in fine siliciclastic facies without the sand-sized bioclasts. Based on these features, together with other sedimentary evidence, *Corumbella* depositional settings in the Tamengo Fm. are reinterpreted as mid-ramp, subtidal settings. The multi-component organization of the skeleton of *Corumbella* favoured disarticulation to yield a sand-sized bioclast, so in turn creating a new complexity to shallow marine clastic settings typical of Phanerozoic marine depositional systems.

1. Introduction

Animals have transformed the planet, transporting matter and energy through biogeochemical cycles, predation and locomotion (Logan *et al.* 1995; Lenton *et al.* 2014). However, even before mobility in marine animals was widespread, they were already capable of altering their host sedimentary environments. Biomineralizing metazoans appeared in the terminal Ediacaran ca. 550 Ma, and the transport and redeposition of derived calcareous bioclasts (Warren *et al.* 2013) can be interpreted as events of redistribution and potentially restructuring of matter (*sensu* Judson, 2017), which generated a new sedimentary grain source in shallow marine carbonate environments (e.g., Warren *et al.* 2013). Here, we present evidence for the physical and chemical substrate redistribution of bioclasts generated by Ediacaran biomineralizing metazoans in siliciclastic settings. The presence of these metazoans thus increased facies heterogeneity and complexity far earlier than previously thought, resulting in a restructuring of this sedimentary factory which persists until today.

Bioclasts in fine-grained siliciclastic rocks can indicate sedimentary processes. Ordovician subtidal bioclastic deposits with a fine matrix indicate storm-induced bioclastic reworking/winnowing of fine sediments and of bioclastic-filled gutter casts (Kreisa, 1981). Bioclastic turbidites can create flow-associated sorting that in turn create more complex textures than their siliciclastic-only counterparts (Bornhold & Pilkey, 1971).

Here, we show that *Corumbella*, an Ediacaran metazoan of problematic affinity, formed bioclastic deposits that record sedimentary dynamics in fine siliciclastic facies of the Tamengo Fm., Brazil. Disarticulated remains of *Corumbella* were reported from carbonate facies from the Tagatiyá Guazú Formation, Paraguay (Warren *et al.* 2011; Warren *et al.* 2012; Warren *et al.* 2017). *Corumbella* has a tubular form, reaching up a few centimetres in length, which has a

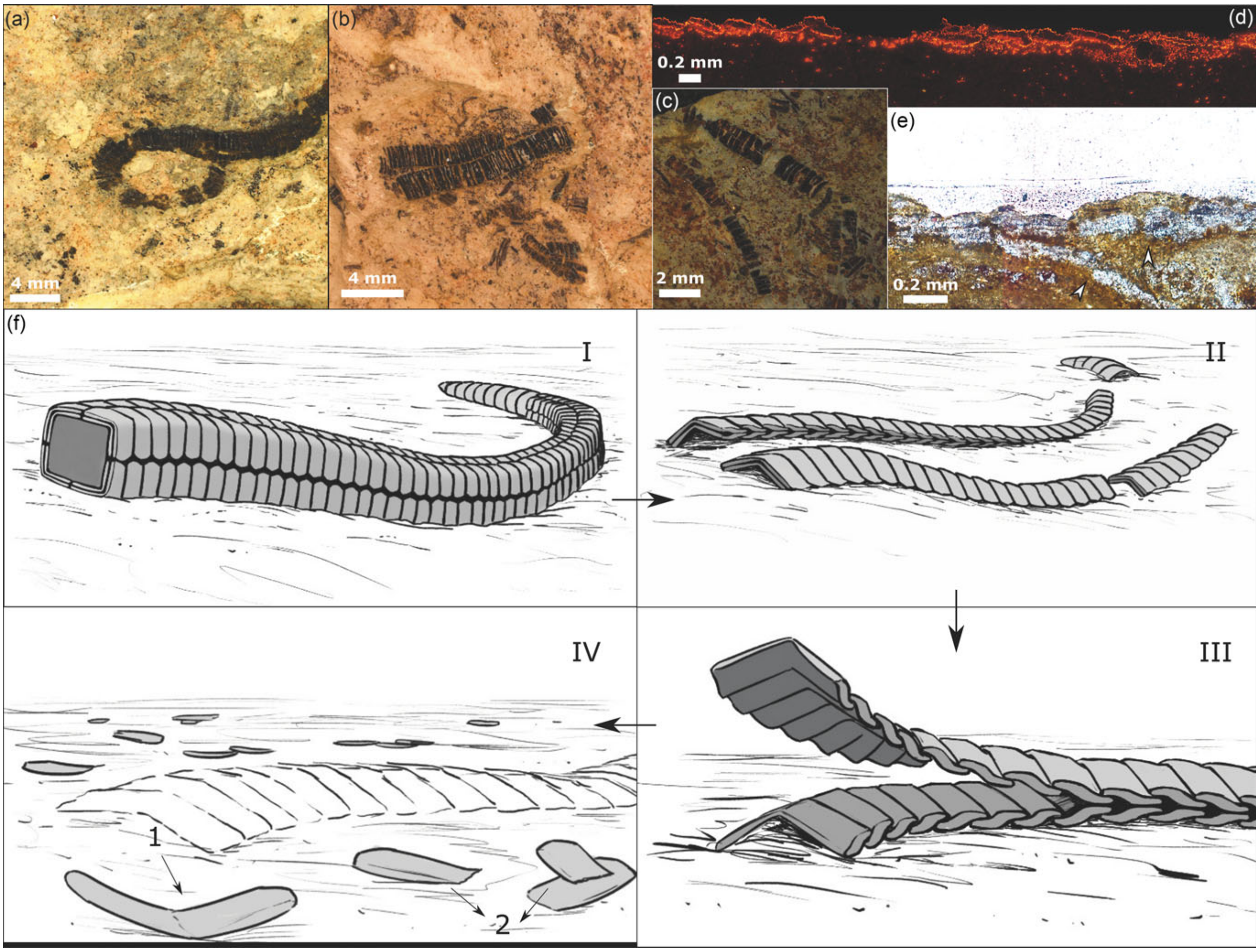

Figure 1. Sequence of disarticulation/fragmentation of *Corumbella* skeleton. Samples: CAP/1A 1024 (a), CAP/1A 1025 (b), CAP/1A 1023 (c and d) and CAP/1F 14 (e). (a) and (f)–I: Articulated sclerites. (b) and (f)-II: Disarticulation along midline. (b), (c) and (f)-II: Disarticulation between consecutive sclerites. (d), (e) and (f)-III: Disarticulation between skeletal layers (arrowheads in E showing wall layers). (b) and (f)-IV: Disarticulation of consecutive sclerites (arrow 1), with fragmentation (arrow 2). Illustrative drawings by Júlia Soares d'Oliveira. Modified from Figs. 2 and S8 of Osés *et al.* (2022).

multi-element skeleton (cataphract) built by originally aragonitic sclerites that can readily disarticulate (Osés *et al.* 2022) (Fig. 1).

2. Geological setting

The Corumbá Group (western Brazil) comprises a mixed siliciclastic-carbonate succession in the South Paraguay Belt, Amazon Craton (Fig. 2; Alvarenga *et al.* 2001). The fossiliferous Tamengo Formation, that outcrops in the cities of Corumbá and Ladário (Mato Grosso do Sul state), comprises mudstones, sandstones and carbonates deposited across a storm-dominated carbonate ramp (Amorim *et al.* 2020). Radiometric dating constrains the deposition of the Tamengo Formation in the interval ca. 555–542 million years old (Parry *et al.* 2017). Here, we concentrate on the siliciclastic levels that outcrop in sections along the Paraguay river (Fig. 2). Shales bearing *Corumbella* were previously interpreted as transgressive hemipelagic sediments (Boggiani, 1997) from outer-ramp settings (Oliveira, 2010; Amorim *et al.* 2020; Ramos *et al.* 2022). Here, these fine-grained clastic facies are reinterpreted as shallow marine, as supported by previous works (Almeida, 1945; Almeida, 1965; Boggiani, 1997; Antunes *et al.* 2023).

3. Materials and methods

Samples were collected in the Sobramil Mine (ELC VI) and in the Cacimba Ecopark (ELC VII), Tamengo Formation, in the cities of Corumbá and Ladário, state of Mato Grosso do Sul, Brazil (Fig. 2). In this study, seven polished slabs and five thin sections were analysed. Fossil samples and thin sections are housed either in the Palaeontological Collections of the Laboratory of Paleobiology and Astrobiology, University of São Carlos (codes CAP/1A and CAP/1F), or of the Institute of Geosciences, University of São Paulo (USP) (code GP/1E).

For microfacies observation, rocks were cut with a diamond saw in the Institute of Astronomy and Geophysics, University of São Paulo (USP). Slabs were serially polished either manually or with progressively finer discs in the Materials Group facilities, Engineering and Technology division of the Brazilian Centre for Research in Energy and Materials. Samples were imaged using either Olympus DSX110 microscope or Zeiss stereomicroscope

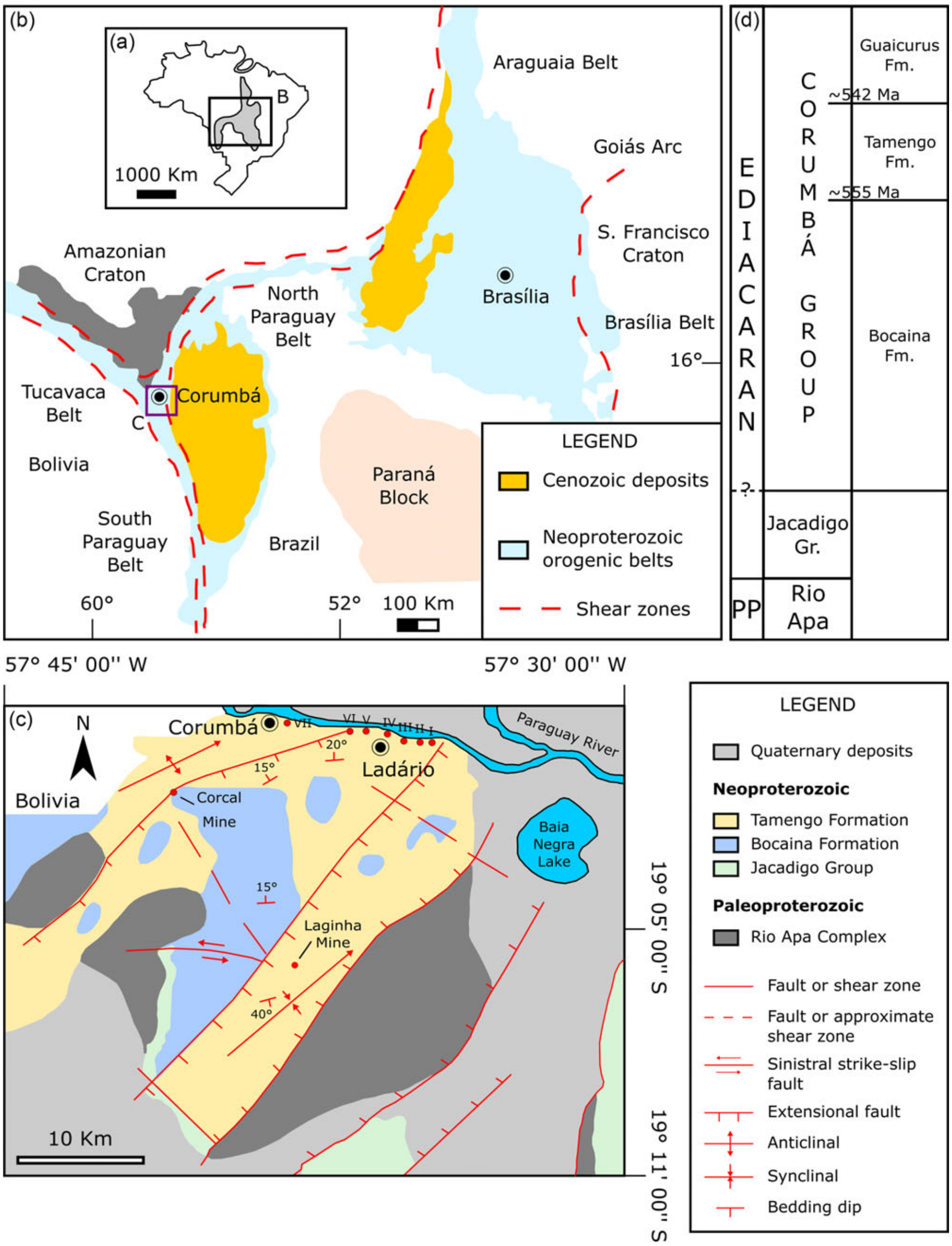

Figure 2. Geological context. (a) Localization of the Tocantins Province in the Brazilian territory. The delimited area highlights the southern-central part of this Province, which is shown in (b). (b) Simplified geological map of the selected area in (a). The delimited area around the city of Corumbá is shown in detail in (c). (c) Geological map of the vicinities of the cities of Corumbá and Ladário, Mato Grosso do Sul state. ELC VI – Sobramil Mine. ELC VII – Cacimba Ecopark. (d) Stratigraphic chart with geological units shown in (c). PP – Palaeoproterozoic. Radiometric ages were published by Parry *et al.* (2017). (a) and (b) were modified from Oliveira *et al.* (2019) (publication "Ediacaran ramp depositional model of the Tamengo Formation, Brazil", Vol. 96, authors: Rick Souza de Oliveira, Afonso César Rodrigues Nogueira, Guilherme Raffaeli Romero, Werner Truckenbrodt, José Cavalcante da Silva Bandeira, Page 102348, Copyright (2019), with permission from Elsevier; https://www.sciencedirect.com/journal/journal-of-south-american-earth-sciences). (c) was modified from Amorim *et al.* (2020) (we acknowledge the authors Kamilla Borges Amorim, Jhon Willy Lopes Afonso, Juliana de Moraes Leme, et al., publication "Sedimentary facies, fossil distribution and depositional setting of the late Ediacaran Tamengo Formation (Brazil)", John Wiley and Sons).

with camera, respectively, in the Laboratory of Palaeobiological Studies and in the Laboratory of Petrographic Microscopy, in the Institute of Geosciences, USP. After the inspection of polished blocks, samples were selected for petrographic thin-sectioning and photographed in an Olympus petrographic microscope with camera.

CL (cathodoluminescence) analysis was done using a Cathodoluminescence Cold Cathode CITL 8200 MK3A coupled with a Nikon microscope (School of GeoSciences, University of Edinburgh). Photomicrographs were taken with a x10 objective lens, current of 900–1000 A and voltage of 25–30 V.

SR-microXRF (synchrotron radiation micro X-ray fluorescence) mapping was performed at the XRF beamline of the Brazilian Synchrotron Light Laboratory (LNLS/CNPEM), following the protocol of Osés *et al.* (2017). PIXE (particle-induced X-ray emission) measurement was performed at the external beam of the LAMFI (Laboratory of Materials Analysis by ionic beams) facilities (Silva *et al.* 2018), at the Institute of Physics, University of São Paulo. The analysis followed the protocol described in Osés *et al.* (2016).

SEM (scanning electron microscopy) analyses were made at the Institute of Geosciences, University of São Paulo, using a FEI Quanta 250 microscope with an Oxford Si(Li) EDS detector. Samples were analysed uncoated. The parameters used can be found in the data bar of each micrograph.

4. Results

In the Sobramil Mine (Figs. 2 and 3), clayey/silty sandstones are associated with black calcareous skeletal fragments (Fig. 4) of *Corumbella* (Fig. 4g) and unidentified calcareous taxa. These bioclasts occur as discontinuous laminae, lenses and pods with erosive sharp basal contacts (Figs. 4, 5a and b). Bioclasts and massive clay form heterolithic structures of planar/undulated/

https://doi.org/10.1017/S0016756824000335 Published online by Cambridge University Press

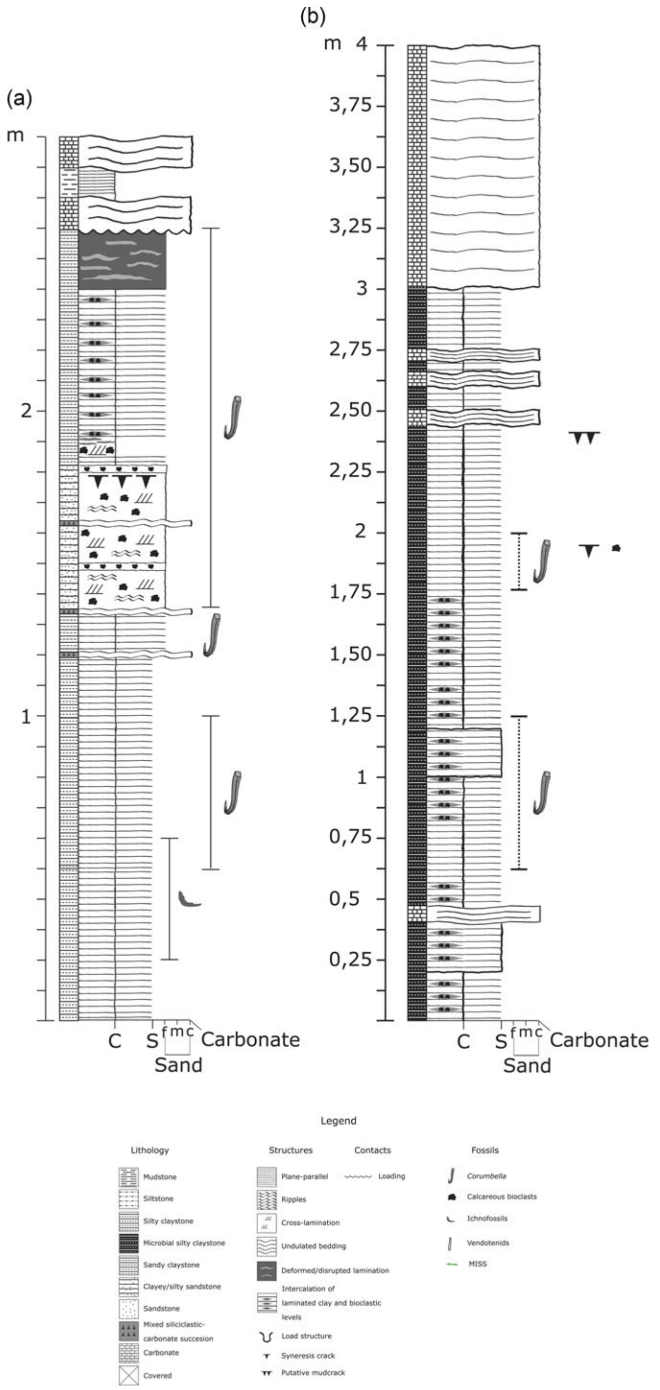

Figure 3. Stratigraphic sections of the sampled outcrops. (a) Sobramil Mine. (b) Cacimba Ecopark. Location in Fig. 2.

wavy horizontal strata with internal plane-parallel lamination and cross-lamination with <1 cm-thick cross-sets (Figs. 4, 5a, b and e). The cross-laminae have low-angle contacts to the cross-strata set boundaries (Figs. 4a and 5e). Ripples are capped by bioclasts and/or iron oxy(hydr)oxides that also subtly follow ripple cross-lamination (Fig. 4i). Thick bioclastic crusts are cut by iron oxy(hydr)oxide partings of pyrite pseudoframboids (Fig. 5a–c). Bioclastic accumulations also form syneresis cracks (Fig. 5f–h). Bioclasts are entrapped in microbial lamination with orientated grains and pyrite pseudoframboids (Fig. 5i–l).

CL (cathodoluminescence) imaging of bioclastic level in Fig. 5a shows that it is formed by calcareous bioclasts with a non-luminescent core and bright luminescent calcite cement (Fig. 6a). SR-microXRF (synchrotron radiation micro X-ray fluorescence) mapping shows the association of calcium to calcareous bioclasts and to cement in these levels (Fig. 6b). Figure 6c and d indicate that the *Corumbella* fossil in Fig. 4g and other bioclasts have a correlation of Ca and of Sr. PIXE (particle-induced X-ray emission) spectrum of a bioclast has high counts of Ca and of Sr relative to the host rock (Fig. 6e).

SEM and EDS (energy-dispersive X-ray spectroscopy) analyses of syneresis cracks in Fig. 5g and h show details of the mineralogy (Fig. 7) and of the composition and cross-cutting relationships of both bioclastic level and clay veins (Fig. 8) forming these structures.

The Cacimba Ecopark has outcrops of dark grey silty/sandy claystone (Figs. 2 and 3). Plane/wavy discontinuous irregular bioclastic laminae/lenses of silt/fine sand forming erosive features (Fig. 9a–c) interlaminate with dark organic wavy-crinkled discontinuous lamination with clay minerals, trapped orientated elongated translucent crystals and pseudoframboids (Fig. 9d–f). V-shaped feature is putative evaporite feature in cross-section (Fig. 9g).

SEM imaging details pyrite framboid in the sample in Fig. 9d–f (Fig. 10a and b). EDS mapping further supports a pyritic composition (Fig. 10c–f). These framboids are associated with organic, microbial, laminae and scattered organic matter (Fig. 10g–k).

5. Discussion

An elemental composition consistent with a calcite mineralogy is shown for bioclasts, as evidenced by SR-microXRF mapping and by PIXE point analysis (Fig. 6b–e). These analyses indicate an association of Sr to Ca-bearing *Corumbella* articulated fossils (Fig. 6c and d) and to the black grains interpreted as bioclasts (Fig. 6c–e). Osés *et al.* (2022) showed that *Corumbella* had a primary aragonitic mineralogy. The bioclasts are black since they are organic-rich (kerogenized), as shown for *Corumbella* fossils by Osés *et al.* (2022). CL imaging of bioclastic levels shows bioclasts as grains with non-luminescent cores that are outlined by bright luminescent margins (Fig. 6a), exactly as shown for *Corumbella* sclerites by Osés *et al.* (2022). This variation in luminescence was attributed by these authors to an increase of Mn and Fe contents towards the margins of the skeletal elements due to recrystallization. CL also shows that the bioclasts are cemented by bright luminescent calcite (Fig. 6a).

The bioclastic deposits are similar to the pre-trilobite, early 'Cambrian shell concentrations' (Li & Droser, 1997), as both are dominated by Small Shelly Fossils (SSFs), <10 cm-thick, and forming discontinuous thin beds and lenses. An increase of deposit thickness later in the Phanerozoic was explained by a decrease of organic content in skeletons, successful colonization of high-energy habitats and increase of carbonate production (Kidwell & Brenchley, 1994).

The absence of many sedimentary features in non-*Corumbella*-hosting clastic sediments of the Tamengo Fm. suggests that an interplay of bioclasts, mud and sedimentary dynamics creates sedimentary complexity. The cataphract organization of *Corumbella* (Osés *et al.* 2022) when disarticulated and fragmented yields bioclasts/crystals that reach very coarse sand grade, up to 2 mm in diameter (Figs. 1 and 4). The predictable disarticulation

https://doi.org/10.1017/S0016756824000335 Published online by Cambridge University Press

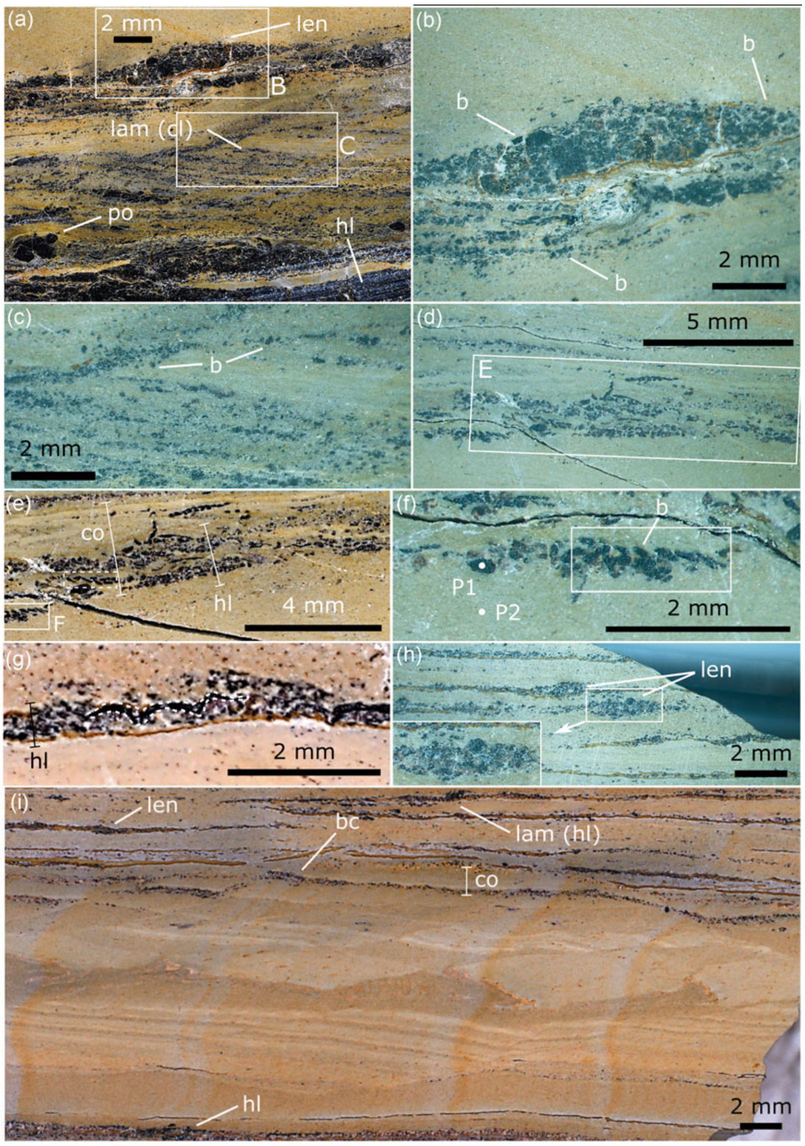

Figure 4. (a)–(i) Polished sections vertical to the lamination. (a)–(i) Interlayering of clay laminae and silt-to-sand horizontal lamination (hl)/laminae (lam), lenses (len) and pods (po) with bioclasts (b), which are delimited by iron oxy(hydr)oxide films (g) and forming cross-lamination (cl) (a). (a) Insets are shown in (b) and in (c). (b) Detail of lens (len) of bioclasts (b). (c) Detail of cross-lamination (cl) formed by bioclasts (b). (d) Bioclastic horizontal lamination with inset shown in (e). (e) Bioclastic horizontal lamination (hl) forming couplets of bioclasts and clay (co). The dashed line rectangle highlights a 'house-of-cards' structure. Inset of another 'house-of-cards' structure is shown in (f). (f) The rectangle highlights the 'house-of-cards' structure formed by bioclasts (b). P1 and P2 locate the PIXE (particle-induced X-ray emission) measurements of Fig. 6e. (g) *Corumbella* fossil with articulating sclerites belonging to a bioclastic horizontal laminae (hl) is delimited by dashed line. (h) Bioclastic lenses (len) with inset showing details of highlighted area. (i) len – lenses; co – couplets of bioclasts and clay; bc – bioclast capping; lam (hl) – horizontal lamination.

behaviour in Fig. 1 (Osés *et al.* 2022) illustrates how progressively smaller unities were formed. Bioclast thickness, microstructure and organic content influence strength, which in turn controls fragmentation (Zuschin *et al.* 2003). A thin skeleton with a possibly laminar microfabric (Osés *et al.* 2022) may have decreased strength in *Corumbella*, presumably in turn increasing fragmentation (Zuschin *et al.* 2003). The multi-element skeleton disarticulation/fragmentation of *Corumbella* yielded variations in grain size and shape that interacted with flow dynamics influencing the geometry, thickness, internal fabrics and sedimentary structures of the deposits. Fine sand-sized bioclasts form <1 mm-thick horizontal discontinuous laminae (Fig. 4e, g and i), thin lenses (Figs. 4i and 5e) and low-angle cross-lamination (Figs. 4a, c and 5e). Flow energy limits the maximum particle size that is transported, and these fine-grained thin deposits formed by lower-energy conditions. The well-sorting of bioclasts forming cross-lamination is explained by current winnowing during ripple formation/migration. Coarse sand-sized bioclasts form ≥2 mm lenses and pods only (Fig. 4a and b). These are local erosive lag deposits – cut-and-fill structures – formed after erosion and flow deceleration (Baas *et al.* 2015). The red films enveloping bioclastic levels bear pyrite pseudoframboids (Fig. 5b and c), representing films that have likely resulted from the decay of biofilms around the deposits.

The heterolithic alternation of bioclasts and massive clay forms by current flow in an upper plane bed regime, which creates sediment 'bursting', followed by deposition of large, heavy bioclasts and clay settling, yielding bioclast/clay fining-upward couplets (Fig. 4d–g) (Cheel & Middleton, 1986). Turbulence explains bioclasts subvertical to the lamination (Fig. 4e). Unequivocal *Corumbella* sclerites (Fig. 4g) have a convex-up configuration and form 'house-of-cards'-like imbrication (Fig. 4e and f), which might indicate tractive flow action (Quaglio *et al.* 2014). The convex-up configuration indicates deposition in high-energy flows (McFarland *et al.* 1999; Yao *et al.* 2016). The variation of thickness of bioclastic-clay couplets might point to periods of longer high-energy conditions – possibly storms with deposit cannibalism (Einsele, 1992) – followed by also long intervals of low-energy deposition (Fig. 4i) vs rapid events (Fig. 4e and g).

Polygonal features with similar orientation and variable sizes have bioclastic accumulations and are here interpreted as syneresis cracks (Fig. 5f). The surface separating part and counterpart –

https://doi.org/10.1017/S0016756824000335 Published online by Cambridge University Press

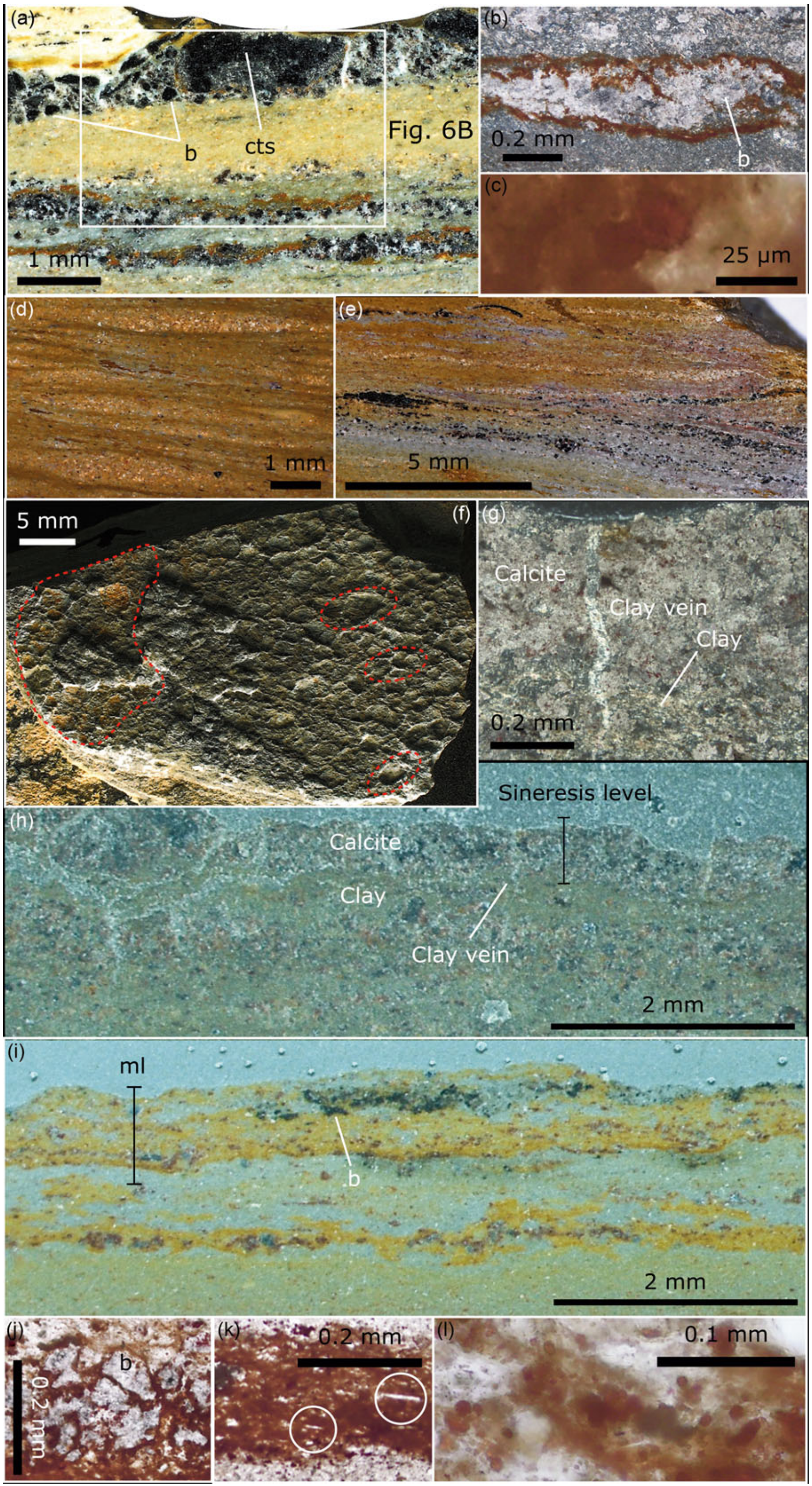

Figure 5. (a), (d)–(f) Polished sections vertical to the lamination. (b), (c), (g)–(l) Thin sections vertical to the lamination. (a) Sample CAP/1A-1059. Crust (top) formed by bioclasts (b). Note a *Corumbella* tube's section (cts). (b) Cross-polarized light (XPL) image of calcareous accumulation delimited by iron oxy(hydr)oxide films with pyrite pseudoframboids (c). (d) Lenticular laminae of fine sand interlayered with clay. (e) Discontinuous irregular laminae and lenses with calcareous sand-sized bioclasts, forming cross-lamination. (f) Negative hyporelief of syneresis cracks. The dashed line oval-shaped drawings highlight some polygonal features of different sizes forming the cracked surface. The area delimited by dashed line has an iron oxy(hydr)oxide veneer. (g) XPL, cut perpendicular to surface in (f) showing silt/sand size anhedral calcite crystals with jigsaw texture, cut by vertical sinuous veins with clay from below. (h) Wider area of thin section in (g). (i)–(l) PPL, sample GP/1E 11175. Microbial lamination (ml) with possible trapped and binded calcareous bioclasts (b), orientated elongated translucent crystals (k) (highlighted by circles), and pyrite pseudoframboids (l).

positive epirelief and negative hyporelief – possesses a reddish iron oxy(hydr)oxide parting (Fig. 5f). In cross-section, the features manifest as an irregular discontinuous thick level of silt/sand-sized anhedral calcite crystals with jigsaw texture (bioclasts), that is interlaminated with clay, and cut by vertical sinuous clay mineral veins that taper downwards (Figs. 5g, h, 7 and 8).

There are several hypotheses for the polygonal features. Load structures can be ruled out since deformation of underlaying clay

https://doi.org/10.1017/S0016756824000335 Published online by Cambridge University Press

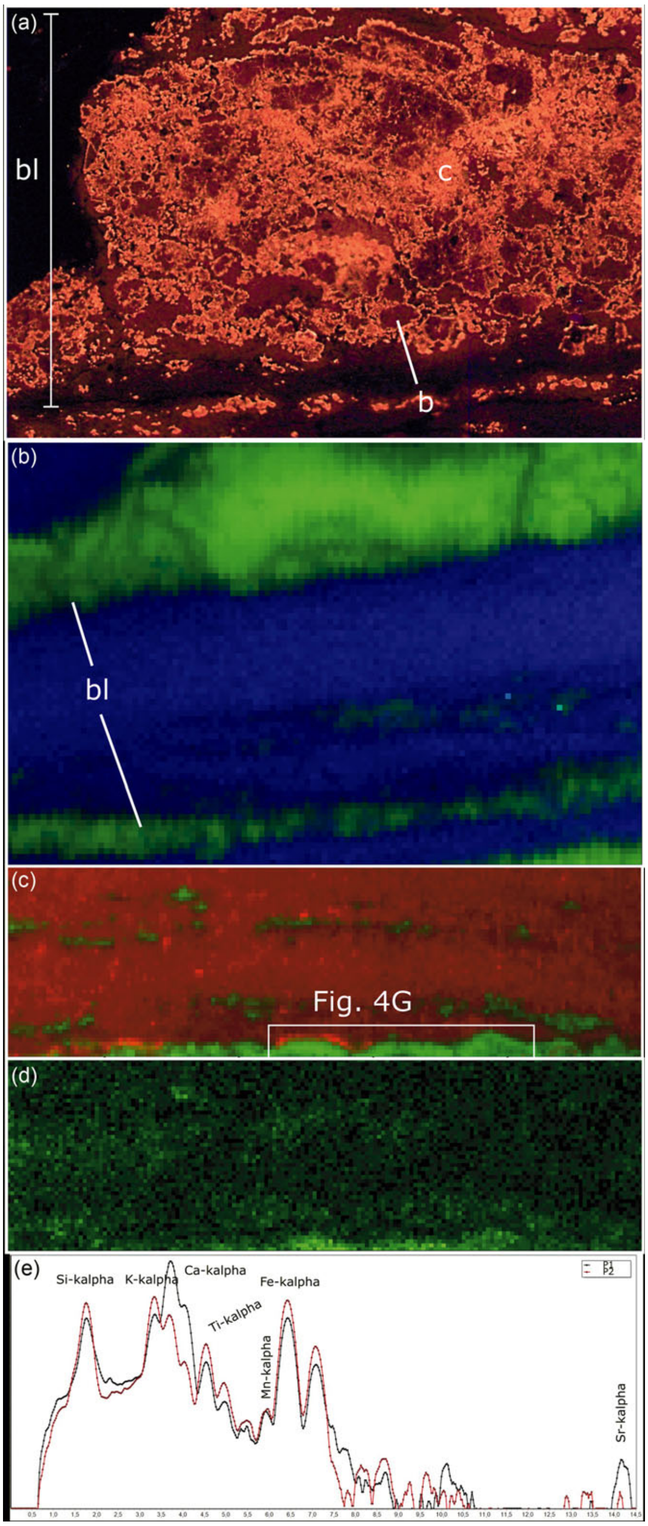

Figure 6. (a) Thin section of sample in Fig. 5a. CL (cathodoluminescence) photomontage showing bioclastic level (bl) formed by calcareous bioclasts (b) with non-luminescent core and bright luminescent calcite cement (c). (b) SR-microXRF (synchrotron radiation micro X-ray fluorescence) map of area delimited in Fig. 5a. Calcium (bioclastic levels (bl)) – green. Potassium (host rock/clay) – blue. (c) and (d) SR-microXRF maps showing bioclastic levels. (c) The delimited area highlights the *Corumbella* fossil in Fig. 4g. Ca – green. Fe – red. (d) Sr map. Note the correlation of Ca (c) and of Sr (d). This indicates that the calcareous bioclasts are Sr-rich. (e) Particle-induced X-ray emission (PIXE) spectra of points P1 (bioclast) and P2 (host rock) marked in Fig. 4f. Note higher counts of Ca and of Sr in the calcareous bioclast.

strata is not observed (Fig. 5g). A MISS origin is undermined by the absence of microbial lamination, organic matter or pseudoframboids associated with the structures (Figs. 5g, 7 and 8). The polygonal features are similar to polygonal desiccation cracks, but no evidence of subaerial exposure has been observed. Molar-tooth structures can also be ruled out since these are more irregular in plane-view and possess ductile and brittle features and vertical crumpled veins infilled with calcite microspar (Pratt, 1998a).

The remaining hypothesis is that the polygonal features are syneresis cracks. Syneresis cracks manifest as lenses or lines with varied shapes (e.g., straight, curved and sigmoidal), with distinct orientations and connection degrees, commonly yielding polygonal shapes and two population sizes at a single bed – ca. 1–10 mm wide and ca. 1–30 cm long (Pratt, 1998). In cross-section, they are vertical/subvertical relative to the horizontal strata, V-shaped, tapering downwards or upwards, and are infilled with silt and sand from overlaying and/or underlaying beds (Pratt, 1998; McMahon *et al.* 2016, and references therein). Syneresis cracks are hosted in marine and non-marine thin strata, finer than fine sand, with clay, silt, sand, and carbonate contribution. They are formed sporadically, underwater, intrastratally in shallow depth, at low-energy settings (Pratt, 1998). Earthquakes trigger sediment dewatering, yielding fluid scape and the formation of distorted dikelets (Pratt, 1998). Syneresis cracks have morphological and dimension similarities with the features herein described, though the latter are shorter, possess clay-infilled veins, and is a mixture of sand-sized bioclasts and cohesive clay deposited under high-energy conditions. The structures herein interpreted as syneresis cracks occur associated with likely bioclastics levels (as observed but not shown by Amorim *et al.* 2020, for the boundary between their silty-shale and calcimudstone), sporadically, both in our bioclastic and microbial microfacies (Figs. 4, 5 and 9), suggesting that bioclasts would have had a role in the formation of such structures. As highlighted by McMahon *et al.* (2016), 'subaqueous sedimentary cracks' need adhesion to yield cracks and these form after some source of stress. In the facies here studied, adhesion could be achieved either by the mixture of clay sediment, organic-rich bioclasts, and water, and/or by the attraction between clay particles (McMahon *et al.* 2016) infilling voids among bioclasts, or even the early cementation (McMahon *et al.* 2016) of calcite around aragonite bioclasts (Osés *et al.* 2022). Additionally, stress could result from the deposition of bioclasts themselves in a stormy context. Amorim *et al.* (2020) attributed syneresis cracks in the Tamengo Formation to a storm-generated origin. A model claimed that rapid deposition over a clay bed would cause dewatering of this deposit, yielding syneresis cracks (see discussion in Pratt, 1998). Here, a model adapted from the model of Pratt (1998) is hypothesized: the turbulent rapid deposition of sand-sized bioclasts mixed with clay during storms caused a seismic shaking-like effect that triggered fissuring (dikelets) and dewatering and fluidization of clay that subsequently filled distorted dikelets. Clay levels below the bioclastic deposit are bent and clay minerals are locally chaotically organized, indicating disturbance. Indeed, the model of Pratt (1998) predicts that the cohesion of clay under the forces of a seismic event yields bending and disruption of clay. It has been proposed that the proportion of swelling clay contribution (smectite) would control the potential of syneresis crack formation (Pratt, 1998). Indeed, syneresis cracks are found in smectite-bearing (Fazio *et al.* 2019) siliciclastic beds of the Tamengo Formation. In sum, bioclastic contribution in the Tamengo Formation siliciclastic settings could have been an

https://doi.org/10.1017/S0016756824000335 Published online by Cambridge University Press

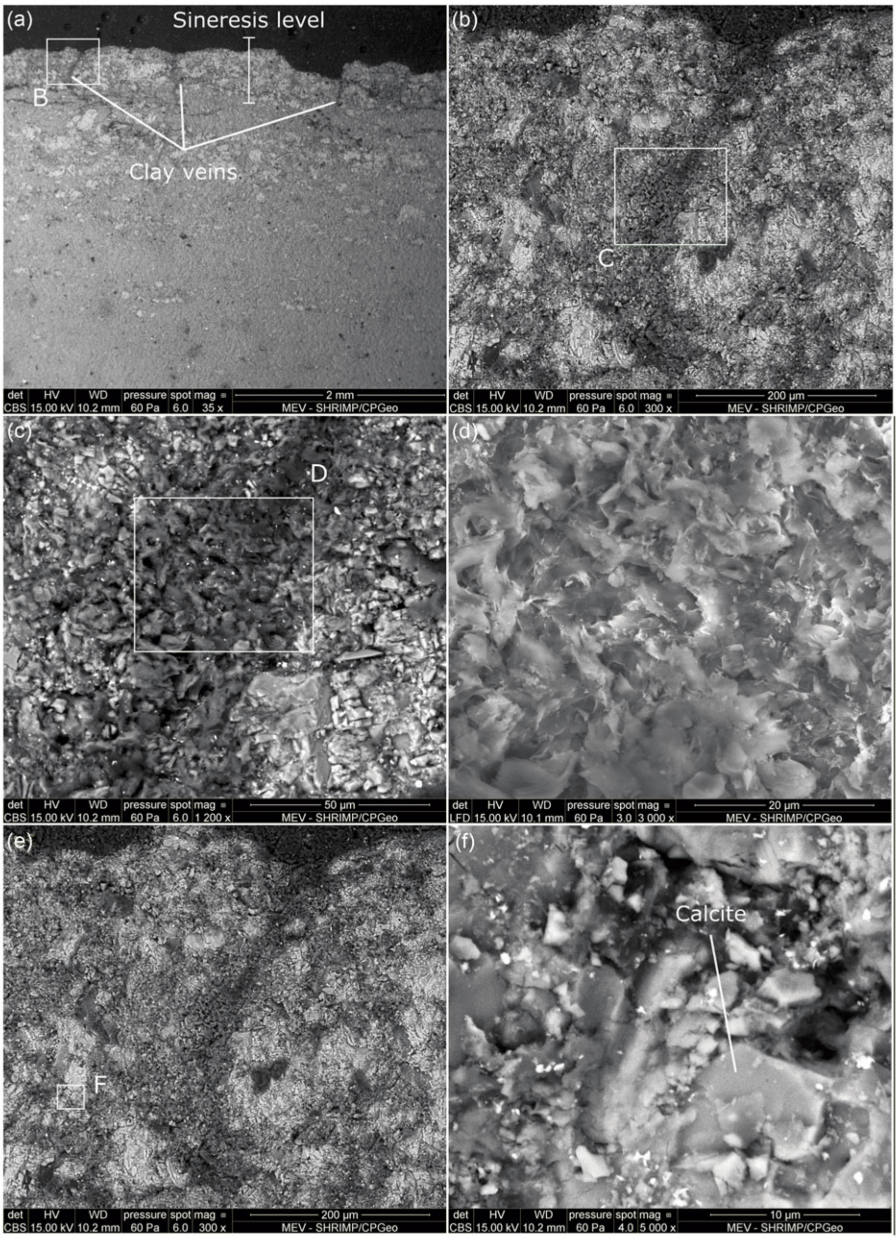

Figure 7. (a)–(c), (e), (f) BSE (backscattered electrons) micrographs of SEM (scanning electron microscopy). (d) SE (secondary electron) micrograph of SEM. (a) Micrograph of thin section in Fig. 5h. (b) Detail of clay vein cutting bioclastic level in (a). (c) Detail of clay vein in (b). (d) Clay minerals in the vein highlighted in (c). (e) Inset delimiting calcite crystals (bioclasts) shown in (f). (f) Calcite crystals forming the bioclasts.

important component of crack structures formed in predominantly cohesive (clayey) sediments.

Ripples are capped by fine sand/silt bioclasts (Fig. 4i). The aragonitic bioclasts (density=2.947 g/cm^3) behaved like heavy minerals (density >2.87 g/cm^3), being swept on an active plane bed, yielding internal dispersive pressures that moved bioclasts to the top of the flow. This creates sorted bioclast concentrations ('lags') over ripple crests (Cheel & Middleton, 1986). Such 'capping' may have prevented underlying bedform erosion.

In heterolithic facies from the Sobramil Mine, microbial mats bearing bioclasts manifest as pyrite pseudoframboids/rare framboids irregular accumulations and orientated elongated translucent crystals (Figs. 5j–l), as these are features of microbial lamination (Schieber, 1999; Noffke *et al.* 2001; Noffke, 2009). Organic-rich, microbial laminae bear pyrite pseudoframboids (Figs. 9d–f and 10g–k). Microbially laminated facies are documented from the Cacimba Ecopark (Fazio *et al.* 2019), and similar lamination occurs lacking bioclasts when interlaminates with erosive features infilled with bioclasts in this locality (Fig. 9). These structures form by current erosion and are filled with sediment and bioclasts during waning energy flow (Pérez-López & Pérez-Valera, 2012).

Bioclastic heterolithic deposits formed in cyclic, fair-weather conditions, under episodic storm disturbance, are considered tide-influenced facies. Lenticular laminae of fine sand interlayered with clay (Fig. 5d) likely formed when sand and clay deposited, respectively, by tidal currents and slack-water (Posamentier & Walker, 2006). Evidence for evaporites (Fazio *et al.* 2019) and desiccation features (Ramos *et al.* 2022) in calcimudstones points to shallow, inter-tidal to supra-tidal deposition. The presence of vendotenids indicates settings with light (Amorim *et al.* 2020). Fazio *et al.* (2019) also described evidence of evaporites in the Cacimba Ecopark, and we show a putative evaporite feature (Fig. 9g) in the dark microbial claystone. Taken together the

https://doi.org/10.1017/S0016756824000335 Published online by Cambridge University Press

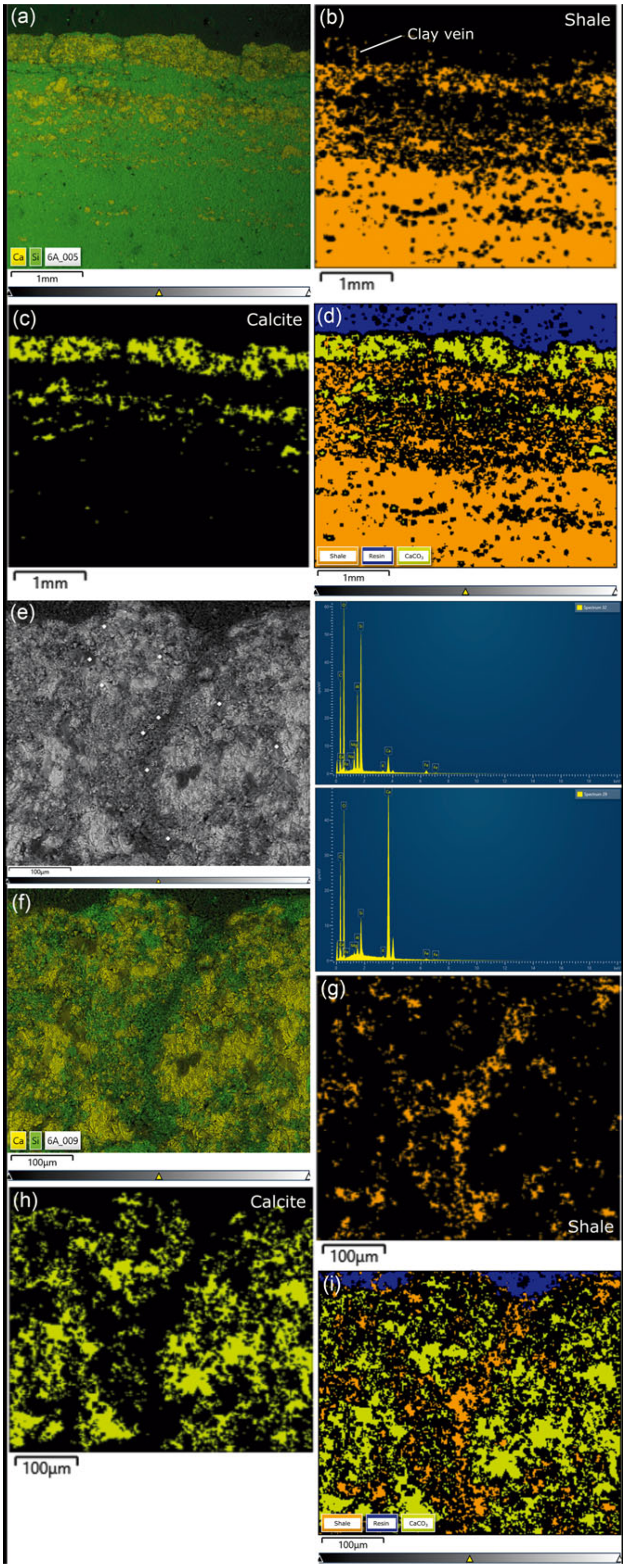

Figure 8. (a) EDS (energy-dispersive X-ray spectroscopy) map of area in Fig. 7a. (b)–(d) Phase analyse maps of area in (a). Note the cross-cutting relationship of clay minerals/shale and the bioclastic calcareous level. (e) SEM-BSE micrograph of area shown in Fig. 7b. EDS measurement points are marked. Selected spectra representative of clay vein (Spectrum 32) and of bioclasts (Spectrum 29) are shown. (f) EDS map of area in (e). (g)–(i) Phase analyse maps of area in (f). Note the cross-cutting relationship of clay minerals/shale and the bioclastic calcareous level.

https://doi.org/10.1017/S0016756824000335 Published online by Cambridge University Press

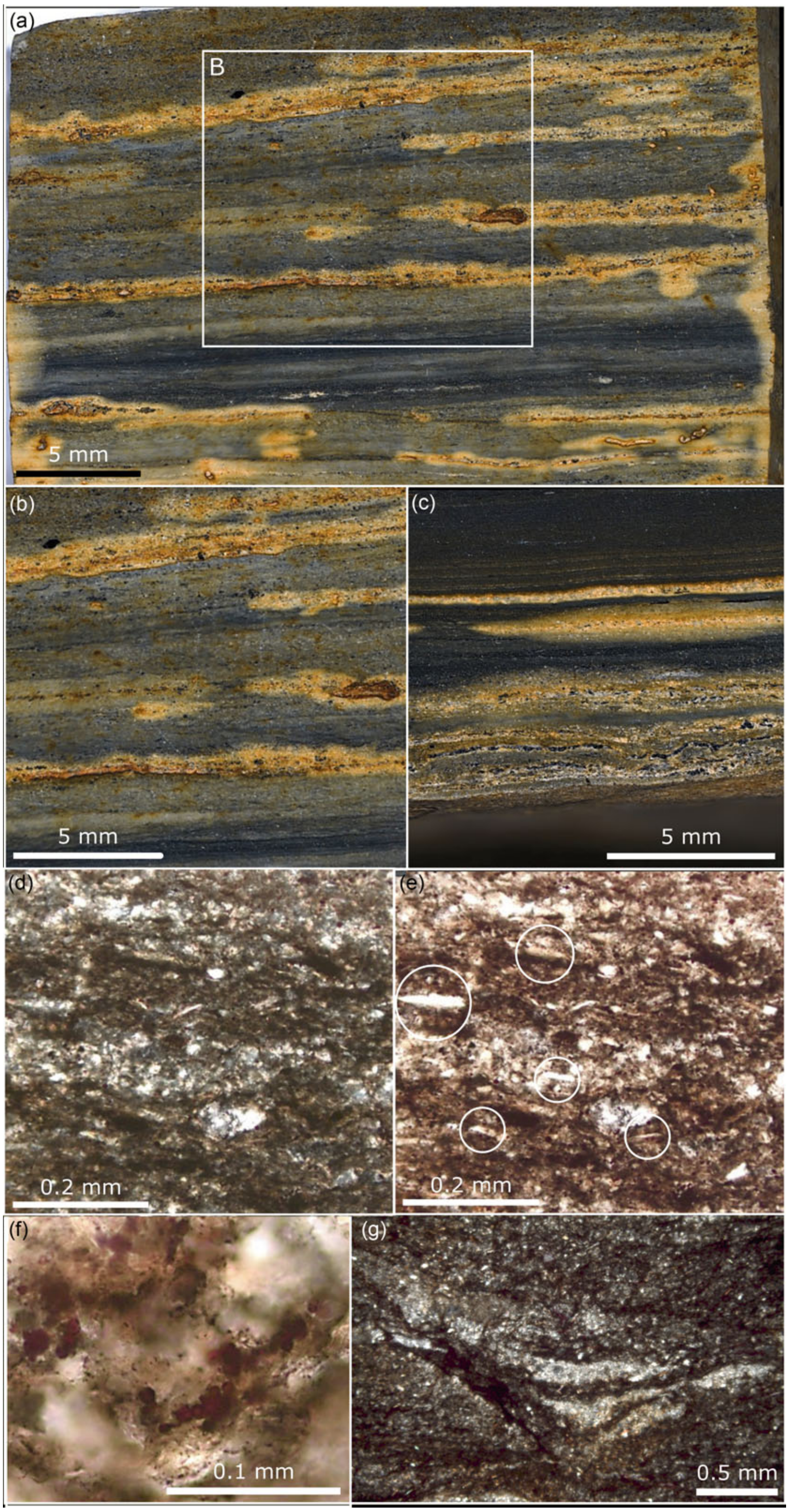

Figure 9. (a)–(c) Polished sections vertical to the lamination. (d)–(g) Thin sections vertical to the lamination. (a)–(c) Plane ((a) and (b)) and wavy (c) discontinuous irregular laminae/lenses of silt/sand with bioclasts (erosive features in (a) and (b)). Plane-parallel tabular laminasets of dark organic clay laminae finely interlayered with silt (top of (c); (d)). (d) (XPL) and (e) (PPL) Silty/sandy/clayey laminae of anastomosing bundles forming wavy-crinkled lamination with organic matter, clay minerals and trapped and orientated elongated translucent crystals. Circles in (e) highlight orientated elongated translucent crystals. (f) (PPL) Close-up of dark laminae in (e), with pyrite pseudoframboids. (g) Putative evaporite structure in cross-section.

evidence of this paragraph, but considering that we have not observed desiccation evidence, we consider that this facies represents deposition in a microbial-dominated, occasionally evaporite protected setting with occasional storm influence, in mid-ramp, subtidal conditions. Previous works associated *Corumbella* with deeper, outer-ramp settings (Oliveira, 2010; Amorim *et al.* 2020; Ramos *et al.* 2022).

Corumbella is found in shallow facies worldwide. In the Tagatiyá Guazú Formation, Paraguay, disarticulated remains of *Corumbella* occurs in thrombolytic mudstones (Warren *et al.* 2011; Warren *et al.* 2017) and in grainstones and massive oolitic grainstones with plane-parallel stratification and wave ripples (Warren *et al.* 2012). The facies from the Tagatiyá Guazú Fm. are interpreted to have been deposited in a shallow carbonate platform,

https://doi.org/10.1017/S0016756824000335 Published online by Cambridge University Press

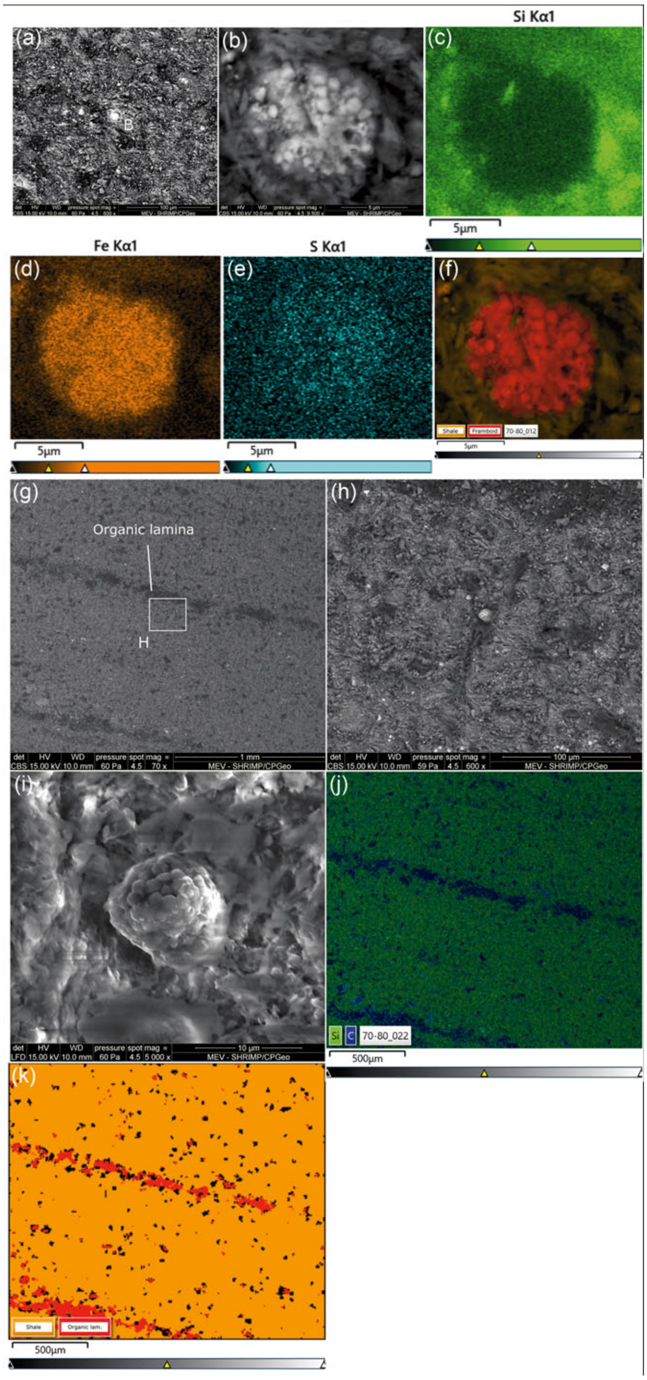

Figure 10. (a), (b), (g), (h) SEM-BSE micrographs. (i) SEM-SE micrographs. (a) and (b) Micrographs of pyrite framboid in the sample in Fig. 9d–f. (c)–(e) EDS maps or area depicted in (b). (f) Phase contrast map of area in (b). (g) Organic (microbial) lamina and scattered organic matter in shale bearing pyrite pseudoframboid shown in (h). (h) Pyrite pseudoframboid nested in an organic-rich spot. (i) Detail of pseudoframboid in (h). (j) EDS map of the area in (g). Note the carbon-rich (organic) microbial laminae. (k) Phase contrast map of area in (g). Organic lam. – organic laminae.

with protected environments, probably in an evaporitic lagoon setting (Warren *et al.* 2012). *Corumbella* is also found in siltstones of the lower member from the Wood Canyon Formation, USA, together with *Gaojiashania* and *Conotubus* (Smith *et al.* 2017). These shales were deposited in a shallow marine setting (Hagadorn & Waggoner, 2000; Smith *et al.* 2017). The Kushk Series of central Iran consists of two facies associations – carbonates deposited in a shallow subtidal setting and shales that represent a deep, outer-ramp environment (Vaziri & Laflamme, 2018). The latter comprises sub-unit 6, consisting of argillaceous grey shales that bear *Corumbella* and other taxa. *Corumbella* was recently reported in fine-grained sandstones of the Huns Member, Urusis Formation, Nama Group (Turk *et al.* 2022).

Afonso *et al.* (2024) showed that the distribution of *Cloudina* calcareous bioclasts in carbonate beds from the Tamengo Fm. are related to sedimentary dynamics. They described two types of shallowing-upward cycles, Type I encompassing proximal mid-ramp deposits with poorly sorted reworked bioclasts and Type II consisting of better-preserved fossils deposited in lower energy conditions at distal mid-ramp and at outer-ramp settings. Afonso *et al.* (2024) and our data reinforce that metazoan bioclasts reflect sedimentary dynamics in the Tamengo Fm., both in carbonate and siliciclastic settings.

The input of calcareous skeletons into siliciclastic sediments also yielded a continuum of dissolution/recrystallization of aragonite as well as decay of skeletal organics. These processes might have led to an increase in carbonate cements and to preservational microbial pathways yielding authigenic mineral precipitation (e.g., pyrite and clay minerals). Osés *et al.* (2022) showed carbonate cements in close association with *Corumbella*.

6. Conclusions

The composition and morphology of the biomineralized metazoan *Corumbella* in the Tamengo Fm. created calcareous, sand-sized sediment in fine siliciclastic beds that in turn added sedimentary complexity. This led to a new interpretation for *Corumbella* depositional settings. Diverse Phanerozoic-style sedimentary features would have hardly been recorded in fine siliciclastic facies without the sand-sized clasts. The shallow marine clastic factory, therefore, underwent this step change in the Late Ediacaran, far earlier than previously thought, with the expansion of biomineralizers to shallow siliciclastic settings. The palaeoenvironmental and palaeobiogeographic distribution of *Corumbella* therefore favours this metazoan as a sedimentary indicator in Late Ediacaran fine siliciclastic facies. Further research could shed light on the geochemical impacts of bioclastic input in siliciclastic sediments in the Late Ediacaran.

Acknowledgements. GLO thanks the Coordination for the improvement of Higher Education Personnel – Brazil (CAPES) – Financing Code 001. GLO thanks the São Paulo research Foundation (FAPESP) for the grants #2017/21584-1, #2021/07007-7, #2016/06114-6, #2022/11586-5, #2023/04501-6, #2022/06485-5, and #2023/14250-0, and the Conselho Nacional de Desenvolvimento Científico e Tecnológico (CNPq) grant #141115/2017-3. GLO thanks the Program of Post-Graduation in Ecology and Natural Resources (São Carlos Federal University), the Program of Post-doctorate and Pesquisador Colaborador, Institute of Physics, University of São Paulo. RW thanks the UKRI NERC Grant NE/T008458/1. We thank the Brazilian Synchrotron Light Laboratory (LNLS/CNPEM) for support during SR-microXRF analyses (proposals 20170831 and 20180422), and the Laboratory of Materials Analysis by ionic beams (LAMFI), Institute of Physics, University of São Paulo. We thank Bruno Becker-Kerber, Esthella Silva, Thibault Le Guelvout and Alessandro Marques for fieldwork support. We thank technical support from Juliana Leme, Ivone Gonzales, Sonia Alonso, Osmar Bagnato, Daniel Kakizaki, Cleber Diniz, Luiz Anelli, Renato Carvalho, Gergely Szabo, Renato Moraes, Amy Shore, John Craven, Douglas Galante, Gustavo Prado, Carlos Pérez and Isaac Sayeg. We thank Júlia d'Oliveira for the illustrations.

Competing interests. The author(s) declare none.

References

Afonso JWL, Pereira LG, de Faria BA, Romero GR, Amorim KB, Basso JML and Trindade RIF (2024) Stratigraphical and sedimentological controls on the distribution of *Cloudina* bioclastic accumulations in the terminal Ediacaran Tamengo Formation (Corumbá Group), Brazil. *Sedimentary Geology* **463**, 106580.

Almeida FFM (1945) Geologia do sudoeste matogrossense. *Boletim da Divisão de Geologia e Mineralogia* **116**, 1–118.

Almeida FFM (1965) Geologia da Serra da Bodoquena (Mato Grosso), Brasil. *Boletim da Divisão de Geologia e Mineralogia, DNPM* **219**, 1–96.

Alvarenga CJS, Moura CAV, Gorayeb PSS and Abreu FAM (2001) Paraguay and Araguaia belts. In *Tectonic evolution of South America* (eds UG Cordani, EJ Milani, AT Filho and DA Campos), pp. 183–193. Brazil: Sociedade Brasileira de Geologia.

Amorim KB, Afonso JWL, Leme JM, Diniz CQC, Rivera LCM, Gómez-Gutiérrez JC, Boggiani PC and Trindade RIF (2020) Sedimentary facies, fossil distribution and depositional setting of the Late Ediacaran Tamengo Formation (Brazil). *Sedimentology* **67**, 3422–3450.

Antunes GC, Warren LV, Okubo J, Freitas BT, Inglez L, Caetano-Filho S and Morais L (2023) Assessing the correlation between Ediacaran-Cambrian units in SW Gondwana: the Tagatiya Guazú (Itapucumi group, Paraguay) and Tamengo (Corumbá Group, Brazil) formations. *Journal of South American Earth Sciences* **130**, 104577.

Baas JH, Best JL and Peakall J (2015) Predicting bedforms and primary current stratification in cohesive mixtures of mud and sand. *Journal of the Geological Society* **173**, 12–45.

Boggiani PC (1997) *Análise Estratigráfica da Bacia Corumbá (Neoproterozoico) – Mato Grosso do Sul*. São Paulo, Brazil: Universidade de São Paulo.

Bornhold BD and Pilkey OH (1971) Bioclastic turbidite sedimentation in Columbus Basin, Bahamas. *Geological Society of America Bulletin* **82**, 1341–1354.

Cheel RJ and Middleton GV (1986) Horizontal laminae formed under upper flow regime plane bed conditions. *The Journal of Geology* **94**, 489–504.

Einsele G (1992) *Sedimentary Basins: Evolution, Facies, and Sediment Budget*. Berlin: Springer-Verlag.

Fazio G, Guimarães E, Walde D, Do Carmo D, Adorno R, Vieira L, Denezine M, Silva C, Viana H, Borges P and Pinho D (2019) Mineralogical and chemical composition of Ediacaran-Cambrian pelitic rocks of The Tamengo and Guaicurus formations, (Corumbá Group - MS, Brazil): stratigraphic positioning and paleoenvironmental interpretations. *Journal of South American Earth Sciences* **90**, 487–503.

Hagadorn JW and Waggoner B (2000) Ediacaran fossils from the southwestern Great Basin, United States. *Journal of Paleontology* **74**, 349–359.

Judson OP (2017) The energy expansions of evolution. *Nature Ecology and Evolution* **1**, 0138.

Kidwell SM and Brenchley PJ (1994) Patterns in bioclastic accumulation through the Phanerozoic: changes in input or in destruction? *Geology* **22**, 1139–1143.

Kreisa DR (1981) Storm-generated sedimentary structures in subtidal marine facies with examples from the middle and upper Ordovician of southwestern Virginia. *Journal of Sedimentary Petrology* **51**, 823–848.

Lenton TM, Boyle RA, Poulton SW, Shields-Zhou GA and Butterfield NJ (2014) Co-evolution of eukaryotes and ocean oxygenation in the Neoproterozoic era. *Nature Geoscience* **7**, 257–265.

Li X and Droser ML (1997) Nature and distribution of Cambrian shell concentrations; evidence from the Basin and Range Province of the Western United States (California, Nevada, and Utah). *Palaios* **12**, 111–126.

Logan GA, Hayes JM, Hieshima GB and Summons RE (1995) Terminal Proterozoic reorganization of biogeochemical cycles. *Letters to Nature* **376**, 53–56.

Mcfarland S, Westrop SR and Cheel RJ (1999) Allogenic versus autogenic processes in the genesis of middle Ordovician brachiopod-rich shell beds, Verulam Formation, Ontario. *Palaios* **14**, 282–287.

Mcmahon S, Hood AVS and Mcilroy D (2016) The origin and occurrence of subaqueous sedimentary cracks. *Geological Society London Special Publications* **448**, 285–311.

Noffke N (2009) The criteria for the biogeneicity of microbially induced sedimentary structures (MISS) in Archean and younger, sandy deposits. *Earth-Science Reviews* **96**, 173–180.

Noffke N, Gerdes G, Klenke T and Krumbein WE (2001) Microbially induced sedimentary structures – a new category within the classification of primary sedimentary structures. *Journal of Sedimentary Research* **71**, 649–656.

Oliveira RS (2010) *Depósitos de rampa carbonática ediacarana do Grupo Corumbá, região de Corumbá, MatoGrosso do Sul*. Belém, Brazil: Universidade Federal do Pará.

Oliveira RS, Nogueira ACR, Romero GR, Truckenbrodt W and Bandeira JCS (2019) Ediacaran ramp depositional model of the Tamengo Formation, Brazil. *Journal of South American Earth Sciences* **96**, 102348.

Osés GL, Petri S, Becker-Kerber B, Romero GR, Rizzutto MA, Rodrigues F, Galante D, da Silva TF, Curado JF, Rangel EC, Ribeiro RP and Pacheco MLAF (2016) Deciphering the preservation of fossil insects: a case study from the Crato Member, Early Cretaceous of Brazil. *PeerJ* **4**, e2756.

Osés GL, Petri S, Voltani CG, Prado GMEM, Galante D, Rizzutto MA, Rudnitzki ID, da Silva EP, Rodrigues F, Rangel EC, Sucerquia PA and Pacheco MLAF (2017) Deciphering pyritization-kerogenization gradient for fish soft-tissue preservation. *Scientific Reports* **7**, 1468.

Osés GL, Wood R, Romero GR, Prado GMEM, Bidola P, Herzen J, Pfeiffer F, Stampar SN and Pacheco MLAF (2022) Ediacaran *Corumbella* has a cataphract calcareous skeleton with controlled biomineralization. *iScience* **24**, 105676.

Parry LA, Boggiani PC, Condon DJ, Garwood RJ, Leme JM, McIlroy D, Brasier MD, Trindade R, Campanha GAC, Pacheco MLAF, Diniz CQC and Liu AG (2017) Ichnological evidence for meiofaunal bilaterians from the terminal Ediacaran and earliest Cambrian of Brazil. *Nature Ecology and Evolution* **1**, 1455–1464.

Pérez-López A and Pérez-Valera F (2012) Tempestite facies models for the epicontinental Triassic carbonates of the Betic Cordillera (southern Spain). *Sedimentology* **59**, 646–678.

Posamentier HW and Walker RG (2006) *Facies Models Revisited*. Tulsa: SEPM Society for Sedimentary Geology.

Pratt BR (1998) Syneresis cracks: subaqueous shrinkage in argillaceous sediments caused by earthquake-induced dewatering. *Sedimentary Geology* **117**, 1–10.

Pratt BR (1998a) Molar-tooth structure in Proterozoic carbonate rocks: origin from synsedimentary earthquakes, and implications for the nature and evolution of basins and marine sediment. *Geological Society of America Bulletin* **110**, 1028–1045.

Quaglio F, Warren LV, Anelli LE, dos Santos PR, Rocha-Campos AC, Gazdzicki A, Strikis PC, Ghilardi RP, Tiossi AB and Simões MG (2014) Shell beds from the Low Head Member (Polonez Cove Formation, early Oligocene) at King George Island, west Antarctica: new insights on facies analysis, taphonomy and environmental significance. *Antarctic Science* **26**, 400–412.

Ramos MEAF, Giorgioni M, Walde DHG, do Carmo DA, Fazio G, Vieira LC, Denezine M, Santos RV, Adôrno RR and Guida LL (2022) New facies model and carbon isotope stratigraphy for an Ediacaran carbonate platform from South America (Tamengo Formation—Corumbá Group, SW Brazil). *Frontiers in Earth Science* **10**, 1–24.

Schieber J (1999) Microbial mats in terrigenous clastics: the challenge of identification in the rock record. *Palaios* **14**, 3–12.

Silva TF, Rodrigues CL, Added N, Rizzutto MA, Tabacniks MH, Mangiarotti A, Curado JF, Aguirre FR, Aguero NF, Allegro PRP, Campos PHOV, Restrepo JM, Trindade GF, Antonio MR, Assis RF and Leite AR (2018) Elemental mapping of largesamples by external ion beam analysis with sub-millimeterresolution and its applications. *Nuclear Instruments & Methods in Physics Research Section B-Beam Interactions with Materials and Atoms* **422**, 68–77.

https://doi.org/10.1017/S0016756824000335 Published online by Cambridge University Press

Smith EF, Nelson LL, Tweedt SM, Zeng H and Workman JB (2017) A cosmopolitan Late Ediacaran biotic assemblage: new fossils from Nevada and Namibia support a global biostratigraphic link. *Proceedings of the Royal Society B: Biological Sciences* **284**, 20170934.

Turk KA, Maloney KM, Laflamme M and Darroch SAF (2022) Paleontology and ichnology of the Late Ediacaran Nasep–Huns transition (Nama Group, southern Namibia). *Journal of Paleontology* **96**, 753–769.

Vaziri SH and Laflamme M (2018) Lithostratigraphy and sedimentary environment of the Precambrian Kushk series of central Iran. *Canadian Journal of Earth Sciences* **55**, 1284–1296.

Warren LV, Fairchild TR, Gaucher C, Boggiani PC, Poire DG, Anelli LE and Inchausti JC (2011) *Corumbella* and in situ *Cloudina* in association with thrombolites in the Ediacaran Itapucumi Group, Paraguay. *Terra Nova* **23**, 382–389.

Warren LV, Pacheco MLAF, Fairchild TR, Simões MG, Riccomini C, Boggiani PC and Cáceres AA (2012) The dawn of animal skeletogenesis: ultrastructural analysis of the Ediacaran metazoan *Corumbella werneri*. *Geology* **40**, 691–694.

Warren LV, Quaglio F, Simões MG, Gaucher C, Riccomini C, Poiré DG, Freitas TB, Boggiani PC, Sial AN and Sial AN (2017) *Cloudina-Corumbella-Namacalathus* association from the Itapucumi Group, Paraguay: increasing ecosystem complexity and tiering at the end of the Ediacaran. *Precambrian Research* **298**, 79–87.

Warren LV, Simões MG, Fairchild TR, Riccomini C, Gaucher C, Anelli LE, Freitas B, Boggiani PC and Quaglio F (2013) Origin and impact of the oldest metazoan bioclastic sediments. *Geology* **41**, 507–510.

Yao L, Aretz M, Li Y and Wang X (2016) Gigantoproductid brachiopod storm shell beds in the Mississippian of South China: implications for their palaeoenvironmental and palaeogeographical significances. *Geologica Belgica* **19**, 1–11.

Zuschin M, Stachowitsch M and Stanton JR (2003) Patterns and processes of shell fragmentation in modern and ancient marine environments. *Earth-Science Reviews* **63**, 33–82.